



Small Molecule Inhibitors of Middle East Respiratory Syndrome Coronavirus Fusion by Targeting Cavities on Heptad Repeat Trimers

Mahmoud Kandeel^{1,2,*}, Mizuki Yamamoto^{3,4}, Abdulla Al-Taher¹, Aya Watanabe⁴, Kentaro Oh-hashii⁵,
Byoung Kwon Park⁶, Hyung-Joo Kwon^{6,*}, Jun-ichiro Inoue^{3,4} and Mohammed Al-Nazawi¹

¹Department of Biomedical Sciences, College of Veterinary Medicine, King Faisal University, Al-Ahsa 31982, Saudi Arabia

²Department of Pharmacology, Faculty of Veterinary Medicine, Kafrelsheikh University, Kafrelsheikh 33516, Egypt

³Research Center for Asian Infectious Diseases, Institute of Medical Science, The University of Tokyo, Tokyo 108-8639,

⁴Division of Cellular and Molecular Biology, Department of Cancer Biology, Institute of Medical Science, The University of Tokyo, Tokyo 108-8639,

⁵Department of Chemistry and Biomolecular Science, Faculty of Engineering, Gifu University, Gifu 501-1193, Japan

⁶Department of Microbiology, Hallym University College of Medicine, Chuncheon 24252, Republic of Korea

Abstract

Middle East Respiratory Syndrome Coronavirus (MERS-CoV) is a newly emerging viral disease with fatal outcomes. However, no MERS-CoV-specific treatment is commercially available. Given the absence of previous structure-based drug discovery studies targeting MERS-CoV fusion proteins, this set of compounds is considered the first generation of MERS-CoV small molecule fusion inhibitors. After a virtual screening campaign of 1.56 million compounds followed by cell-cell fusion assay and MERS-CoV plaques inhibition assay, three new compounds were identified. Compound numbers 22, 73, and 74 showed IC₅₀ values of 12.6, 21.8, and 11.12 μM, respectively, and were most effective at the onset of spike-receptor interactions. The compounds exhibited safe profiles against Human embryonic kidney cells 293 at a concentration of 20 μM with no observed toxicity in Vero cells at 10 μM. The experimental results are accompanied with predicted favorable pharmacokinetic descriptors and drug-likeness parameters. In conclusion, this study provides the first generation of MERS-CoV fusion inhibitors with potencies in the low micromolar range.

Key Words: MERS-CoV, Antiviral agents, Virtual screening, Plaques inhibition

INTRODUCTION

Middle East Respiratory Syndrome Coronavirus (MERS-CoV) is an emerging viral disease comprised of complex symptoms with a fatal outcome (Rahman and Sarkar, 2019). MERS-CoV is considered a zoonotic disease due to inclusion of potential animal hosts (Chan *et al.*, 2015). Additionally, human-to-human transmission further aggravates the severity of the virus (Memish *et al.*, 2013; Kim *et al.*, 2016). The increasing number of MERS-CoV infected cases over several years suggests the worsened virulence and adaptation of the virus to several species over a wide geographic distribution (Su *et al.*, 2015; Cho *et al.*, 2016). Due to the lack of effective treatment to combat MERS-CoV infection, there is an urgent need for the discovery of new drugs against this virus.

Interaction of the virus spike with host cell receptor is the forerunner of viral membrane fusion (Bosch *et al.*, 2003). The MERS-CoV spike is composed of subunits S1 and S2. The N-terminal S1 is responsible for binding with the host cell receptor dipeptidyl peptidase-4 (DPP4) (Wang *et al.*, 2013; Kandeel *et al.*, 2014). Subunit S2 concerns the fusion protein and accomplishes the fusion process via several structural rearrangements. Host proteases, such as transmembrane protease serine 2 (TMPRSS2) and cathepsins, control the cleavage of S1 to expose S2 subunit (Yamamoto *et al.*, 2016). The S2 subunits consist of protein heptad repeat domains 1 and 2 (HR1 and HR2), where a homotrimer with three exposed hydrophobic pockets is formed on the surface of HR1 (Xia *et al.*, 2014). These pockets act as a receptacle for HR2 during viral fusion (Gao *et al.*, 2013). The movement of HR2 toward

Open Access <https://doi.org/10.4062/biomolther.2019.202>

This is an Open Access article distributed under the terms of the Creative Commons Attribution Non-Commercial License (<http://creativecommons.org/licenses/by-nc/4.0/>) which permits unrestricted non-commercial use, distribution, and reproduction in any medium, provided the original work is properly cited.

Received Dec 2, 2019 Revised Jan 13, 2020 Accepted Jan 23, 2020

Published Online Mar 4, 2020

*Corresponding Authors

E-mail: mkandeel@kfu.edu.sa (Kandeel M), hjookwon@hallym.ac.kr (Kwon HJ)

Tel: +966-568918734 (Kandeel M), +82-33-248-2635 (Kwon HJ)

Fax: +966-13-589-6617 (Kandeel M), +82-33-241-3640 (Kwon HJ)

its binding site on HR1 increases the proximity between viral and cell membranes to initiate the fusion process.

Several studies on developing MERS-CoV fusion inhibitors have detected protein fragments and small molecules from high throughput screening (Sun *et al.*, 2017; Wang *et al.*, 2018; Huang *et al.*, 2019). However, structure-based research targeting the MERS-CoV fusion protein is lacking. To the best of our knowledge, this is the first study reporting the discovery of small MERS-CoV fusion inhibitors based on a predefined structure on the surface of MERS-CoV S2 fusion proteins. The aim of this work includes: 1) mapping druggable pockets on the surface of HR1; 2) targeting the pocket hosting HR2 helix (P_{HR2}) on the surface of HR1; 3) virtual screening and drug discovery studies of potential MERS-CoV fusion inhibitors; and 4) testing the new compounds in the inhibition of cell-cell fusion as well as MERS-CoV plaque formation assays. The discovered compounds, interacting with cavities on the surface of HR1, are expected to interfere with HR2 recognition on HR1 and the production of a malformed fusion complex. The compounds discussed here are considered the first generation of MERS-CoV structure-based fusion inhibitors, providing a promising basis for future anti-MERS-CoV drug discovery studies.

MATERIALS AND METHODS

Construction of compounds dataset and ligand preparation

A subset of compounds was constructed from two screening libraries, including the core library of Chembridge (San Diego, CA, USA) comprised of 1.2 million compounds and the HTS library from Life Chemicals (Niagara-on-the-Lake, Canada) comprised of 360,000 compounds. All compounds were 3D optimized by Ligprep software using OPLS2005 force field and saved in SDF format. The designated number of compounds contained multiple conformations, which were pre-screened before docking to exclude high-energy conformers.

Drug-likeness and ADME pharmacokinetic descriptors predictions

The pharmacokinetic properties and drug-likeness descriptors, including Lipinski's rule of five, were predicted by Qikprop v4.2 (Schrödinger, LLC, NY, USA). The selected descriptors include molecular weight, hydrogen bond acceptor, hydrogen bond donor, oral absorption % in humans, number of violations of Lipinski's rule of five, predicted octanol/water partition coefficient (QPlogP o/w), predicted aqueous solubility (QPlogS), number of rotatable bonds, predicted IC_{50} value for blockage of HERG K⁺ channels (QPlogHERG), apparent Caco-2 cell permeability, predicted brain/blood partition coefficient, predicted skin permeability (QPlogKp), predicted apparent MDCK cell permeability, binding to human serum albumin, total solvent accessible surface area, and hydrophilic component of the SASA. The predicted compounds toxicity and carcinogenicity was implemented in the preADMET web based application (<https://preadmet.bmdrc.kr/>).

MERS-CoV S2 fusion protein preparation

The MERS-CoV fusion core structure of the S2 protein was retrieved from the protein data bank (PDB ID 4NJL), which contains a trimer of the fusion core. 4NJL was optimized for docking and virtual screening by using the protein preparation

module in Maestro software package (Schrödinger, LLC). The undesirable water molecules and crystallographic compounds were removed. Then, the protein was protonated to add polar hydrogens, and the structure was optimized and minimized using OPLS2005 force field.

Identification of drug-binding cavities

During the viral fusion process, HR2 comes into contact with a binding groove on HR1. The principle in finding cavities is to identify a druggable site on the surface of HR1 and define it as a receptor, then find a chemical molecule that theoretically matches this site. At a certain time during viral fusion, the expected compound attaches to the HR1 cavity and might interfere with proper recognition of HR2. To perform this task, two approaches were implemented. First, MERS-CoV HR1 was extracted in its fusion state and mapped by the SiteMap (druggable pockets search tool) module in Schrodinger suite. The top ranked potential binding sites were set to contain at least 15 site points per detected site. The produced top five cavities were inspected regarding their size, substructure components, hydrogen bond donors and acceptors, presence of hydrophobic and charged residues, as well as surface availability. The predicted druggable pockets were identified as P₁, P₂, P₃, P₄ and P₅. In the second approach, the cavity hosting the central helix of HR2 is targeted (Fig. 1A). Because most of the strong peptide HR2 analogues comprise this helical component of HR2, small molecules mimicking this structure were examined in this study. The cavity hosting HR2 helix on the surface of HR1 was studied via virtual screening to find potential strong binding molecules. This cavity was identified as P_{HR2}. The optimized and protein prepared structure was used in a brief molecular dynamics (MD) simulation to remove any clashes or bumps. The MD simulation was performed as previously described (Kandeel *et al.*, 2018).

Virtual screening

Docking grids were constructed separately for P₁, P₂, and P_{HR2}. Grid boxes were generated by selecting x, y, z coordinates at the center of each cavity with a grid box size of 15 Å (Fig. 1A). The grid generation was adopted by using the Maestro grid generation module. In order to obtain accurate docking runs, the Schrodinger glide docking module was set to standard precision (SP docking) (Friesner *et al.*, 2004; Halgren *et al.*, 2004). To decrease the penalties of close contacts and simulate the flexibility of the protein site, the Van der Waals radius-scaling factor was set to 0.8. The Chembridge core library was divided into sets of 100,000 compounds in a total of 12 sets, and the life chemicals HTS library was divided into sets of 30,000 compounds; all sets were run on a cluster of PCs. The output files were retrieved, and a new pool comprised of compounds with docking scores of -8.00 or higher was constructed.

The top compounds from the first run were used in the second stage docking using the extra precision module (XP docking) in Glide software. XP docking is thought to remove the false positive during SP docking. The selected compounds with docking scores of -8.0 or higher were visually inspected for their binding mode, pocket-filling pattern, and interactions with the pocket residues. Finally, a set of 88 compounds were purchased for lab assays (Supplementary Table 1). All compounds exhibited confirmed purity of ≥95%.

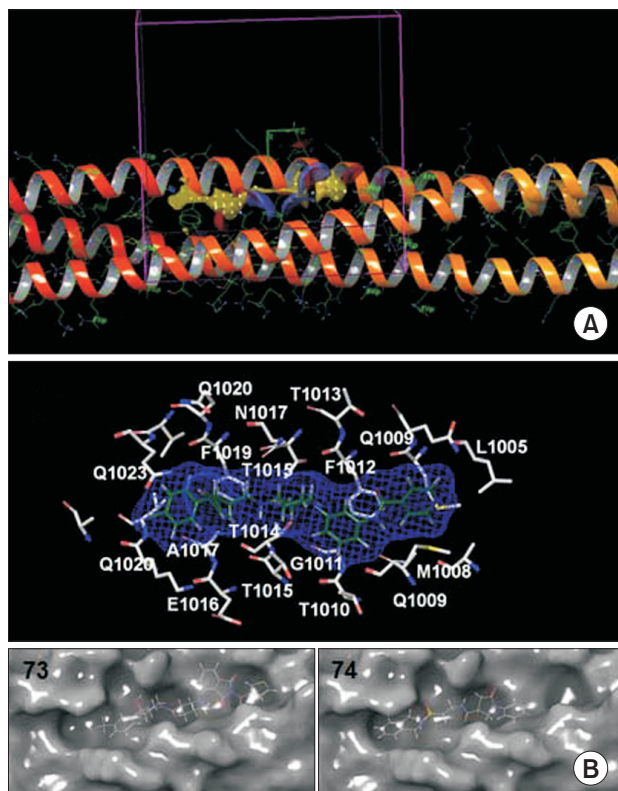


Fig. 1. The site of docking on MERS-CoV HR domains. (A) The druggable pocket of HR2 predicted by SiteMap software. Hydrogen bond donors in blue, acceptors in red and hydrophobic locations is in yellow. The docking grid box is in purple colour. (B) The composition of HR2 binding pocket. The docked compound in green was included in blue surface mesh. The MERS-CoV residues names and numbers are in white colour. The position of compounds 73 and 74 within the binding pocket is provided with MERS-CoV HR1 is surrounded by a molecular surface.

Cell-cell fusion assay

The cell-cell fusion assay was performed as described previously (Yamamoto *et al.*, 2016). To quantitate the cell-cell fusion, a pair of 293FT-based reporter cells, effector and target cells, that express individual split reporters (DSP1-7 and DSP8-11 proteins) were used, because DSP1-7 and DSP8-11 produce fluorescence and luminescence only when the two proteins form a tight complex (Wang *et al.*, 2014). The effector cells stably expressing DSP8-11 and S-protein and the target cells stably expressing DSP1-7 together with CD26 and TMPRSS2 were prepared. 2 h before the fusion assay, both cells were treated with 6 μ M EnduRen (Promega, Madison, WI, USA), a substrate for Renilla luciferase, to activate EnduRen. 1 mL of each compound dissolved in dimethyl sulfoxide (DMSO) was added to 384-well plates (Greiner Bioscience, Frickenhausen, Germany) using a 12-stage workstation (Biotech, Tokyo, Japan). Next, a Multidrop dispenser (Thermo Scientific, Waltham, MA, USA) was used to add 50 μ L of each single cell suspension (1.5×10^4 effector and target cells) to the wells. Incubation was performed at 37°C for 4 h, then RL activity measurements were obtained with a microplate reader (PHERAStar Plus, BMG Labtech, Cary, NC, USA).

MERS-CoV plaque formation assay

African green monkey kidney cells (Vero cells) were purchased from the American Type Culture Collection (ATCC, Manassas, VA, USA). The cell culture was kept in a CO₂ incubator at 37°C in Dulbecco's modified Eagle's medium (DMEM, Thermo Fisher Scientific, Waltham, MA, USA) containing 10% fetal bovine serum (FBS, Thermo Fisher Scientific), 25 mM HEPES, 100 U/mL penicillin and 100 μ g/mL streptomycin in. MERS-CoV was obtained from the Korea Centers for Disease Control and Prevention (CoV/KOR/KNIH/002_05_2015, Permission No. 1-001-MER-IS-2015001).

A total of 15 compounds from two experimental sets was used in the plaque reduction assay. The first set was from the top 10 compounds showing the highest docking scores including compounds no. 22, 74, 73, 75, 4, 76, 58, 54, 35 and 78 and 5 compounds suggested from cell-cell fusion assay including compounds no. 60, 61, 69, 26, and 33 (Table 1). The plaque reduction assay was performed as reported previously (Park *et al.*, 2019). Vero cells were cultivated on six-well plates for 12 h at 6×10^5 cells/well. MERS-CoV was mixed with each compound at a final concentration of 10 μ M for 30 min at 37°C. The mixtures of MERS-CoV and each compound were treated to Vero cells in each well and then incubated for 1 h. After incubation, the supernatants were removed and DMEM/F12 medium (Thermo Fisher Scientific) containing 0.6% oxid agar was transferred to each well. 4 days after infection, plaque formation was observed by staining with crystal violet and plaque numbers were counted.

Cytotoxicity assays in human embryonic kidney and Vero cells

Human embryonic kidney cells 293 (HEK293 cells) were maintained in Dulbecco's modified Eagle's minimum essential medium containing 5% fetal bovine serum. For the detection of cell viability based on mitochondrial activity, HEK293 cells (1×10^4 cells/100 μ L) in a 96-well plate were treated with the indicated compounds at 20 μ M or vehicle (DMSO) for 25 h. For the final 2 h, each well was treated with WST01 solution (Dojindo) and incubated at 37°C. Cell viability was determined based on the difference between absorbance at 450 and 620 nm as an indicator, according to a previous study (Oh-hashii *et al.*, 2018).

Vero cells (1×10^3 cells/well) were plated on 96-well plates and cultured for 12 h. The cells were treated with compound C73 or C74 at the indicated concentrations or with 10% dimethyl sulfoxide (DMSO) as a control for 3 days. Then, cells were treated with 3-(4,5-dimethylthiazol-2-yl)-2,5-diphenyltetrazolium bromide (MTT, Sigma-Aldrich, St. Louis, MO, USA) for 4 h at 37°C. The formazan crystals were dissolved in DMSO, and the absorbance at 570 nm was measured using a microplate reader (Thermo Fisher Scientific, Ratastie, Finland). In this assay, the two compounds, 22 and 73, with improved plaque inhibition scores were used.

Statistical analysis

Correlation between the docking score, plaque formation and cell-cell fusion assay was performed by GraphPad Prism (GraphPad Software, San Diego, CA, USA) using Pearson's correlation coefficient.

Table 1. Chemical structure of compounds and their inhibitory properties on MERS-CoV using plaques inhibition assay. The values represent the average from three different cultures. Cell viability measurement was based on mitochondrial activity

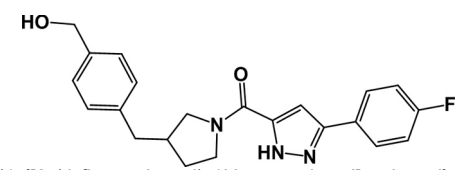
Compound no	ID	Chemical name	Total plaque No.	% Plaque	Cytotoxicity against HEK cells
22	24071746	PBS	568	117.4	0.596
		10% DMSO	484	100	
			268	55.3	
74	F2282-0127*	{4-[(1-[[3-(4-fluorophenyl)-1H-pyrazol-5-yl]carbonyl]pyrrolidin-3-yl)methyl]phenyl}methanol	172	35.5	0.568
73	98931397	1-(4-chlorophenyl)-N-(2-((3,4-dihydroisoquinolin-2(1H)-yl)sulfonyl)ethyl)-5-oxopyrrolidine-3-carboxamide	212	43.8	0.602
75	F2282-0124*	4-[3-({4-hydroxy-4-[3-(trifluoromethyl)phenyl]-1-piperidinyl}carbonyl)-1-piperidinyl]-2-(3-thienylmethyl)-1H-isoindole-1,3(2H)-dione	332	68.6	0.604
4	6505627	N-(2-((3,4-dihydroisoquinolin-2(1H)-yl)sulfonyl)ethyl)-5-oxo-1-(p-tolyl)pyrrolidine-3-carboxamide	316	65.3	0.603
76	F2282-0128*	4-(1,3-dioxo-1,3-dihydro-2H-isoindol-2-yl)-N-2-naphthylbutanamide	276	57.0	0.520
		N-(2-((3,4-dihydroisoquinolin-2(1H)-yl)sulfonyl)ethyl)-1-(3,4-dimethylphenyl)-5-oxopyrrolidine-3-carboxamide			

Table 1. Continued 1

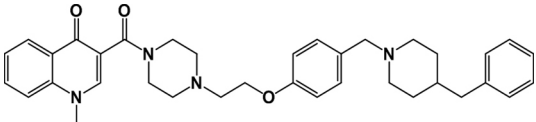
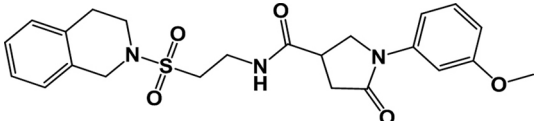
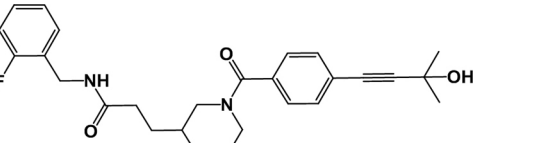
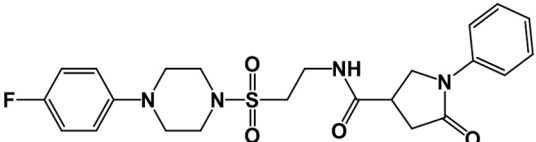
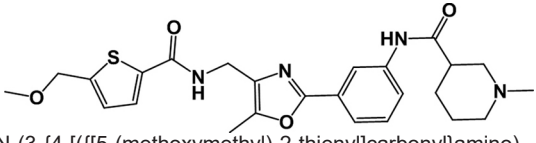
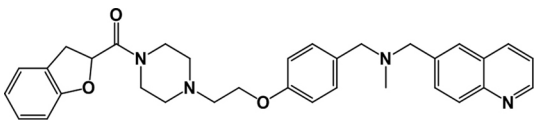
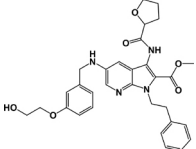
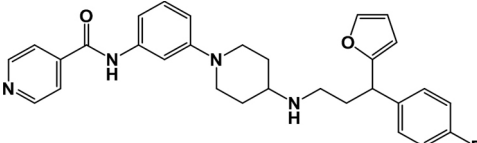
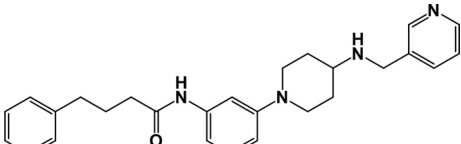
Compound no	ID	Chemical name	Total plaque No.	% Plaque	Cytotoxicity against HEK cells
58	57295921	 3-[[4-(2-[[4-(4-benzyl-1-piperidinyl)methyl]phenoxy]ethyl)-1-piperazinyl]carbonyl]-1-methyl-4(1H)-quinolinone	304	62.8	0.602
77	F2282-0139*	 N-(2-((3,4-dihydroisoquinolin-2(1H)-yl)sulfonyl)ethyl)-1-(3-methoxyphenyl)-5-oxopyrrolidine-3-carboxamide	392	81.0	0.578
35	30625545	 N-(2-fluorobenzyl)-3-{1-[4-(3-hydroxy-3-methyl-1-butyn-1-yl)benzoyl]-3-piperidinyl}propanamide	368	76.0	0.580
78	F2068-0373	 N-(2-((4-(4-fluorophenyl)piperazin-1-yl)sulfonyl)ethyl)-5-oxo-1-phenylpyrrolidine-3-carboxamide	396	81.8	0.574
26	25947446	 N-(3-(4-(((5-(methoxymethyl)-2-thienyl)carbonyl)amino)methyl)-5-methyl-1,3-oxazol-2-yl)phenyl)-1-methyl-3-piperidinecarboxamide	468	96.7	0.587
60	66172782	 (4-{2-[4-(2,3-dihydro-1-benzofuran-2-yl)carbonyl]-1-piperazinyl]ethoxy}benzyl)methyl(6-quinolinyl)methylamine	452	93.4	0.572
69	78170314	 methyl 5-[[3-(2-hydroxyethoxy)benzyl]amino]-1-(2-phenylethyl)-3-[(tetrahydro-2-furanylcarbonyl)amino]-1H-pyrrolo[2,3-b]pyridine-2-carboxylate	388	80.2	0.529

Table 1. Continued 2

Compound no	ID	Chemical name	Total plaque No.	% Plaque	Cytotoxicity against HEK cells
61	67801543	 N-[3-(4-[[3-(4-fluorophenyl)-3-(2-furyl)propyl]amino]-1-piperidinyl)phenyl]isonicotinamide	316	65.3	0.173
33	29194995	 4-phenyl-N-(3-{4-[(3-pyridinylmethyl)amino]-1-piperidinyl}phenyl)butanamide	412	85.1	0.588

*Compounds purchased from Life Chemicals Inc (Niagara-on-the-Lake, Canada). The rest of compounds were purchased from Chembridge (San Diego, CA, USA).

RESULTS

Assignment of druggable sites by SiteMap

Using SiteMap software (Schrödinger, LLC), the top 5 predicted cavities were examined. Pocket numbers 1-5 displayed total areas of 1970, 1060, 1100, 968, and 679 Å², respectively. For virtual screening studies, only P₁ and P₂ were used. The other three pockets were excluded due to the similarity of P₃ with P₂, small cavity volumes of P₄ and P₅, and surface inaccessibility of P₅.

Virtual screening

The structure of MERS-CoV S2 fusion protein was prepared for virtual screening. Two approaches were used to deliver the expected compounds, which included cavity filling and HR2 helix replacement. In the former approach, HR1 was mapped by SiteMap software to find the top 5 druggable pockets. In the latter approach, the cavity hosting HR2 on the surface of HR1 was used to find suitable compounds to fill this cavity (Fig. 1). A compound library was constructed comprising 1.56 million compounds from two commercial sources. For retrieval of results, docking score cut off was used and compound selection was based on a docking score of -8.0 or higher. Via SP docking, about 256 compounds produced docking scores of -8.0 or higher. This set was redocked using XP docking to obtain the final 88 compounds (Supplementary Table 1). Within this set, 6 compounds scored a value of -8.0 or higher with P₁, including compounds 2, 12, 26, 81, 82, and 83, while compounds 24 and 59 had the same score as P₂. The rest of the compounds were docked into P_{HR2}. All 88 compounds were used in the cell-cell fusion assay, while the top 10 compounds with highest docking scores were used in the MERS-CoV plaque formation assay in addition to 5 compounds suggested from the results of the cell-cell fusion assay.

The structure of MERS-CoV heptad repeat trimers is comprised of three HR1 and three HR2 helices. Each HR2 helix is placed in the cavity between two adjacent HR1 helices. The

interaction of compounds with P_{HR2} contains a combination of hydrophobic and hydrogen bonding interactions. The P_{HR2} pocket is lined by hydrophobic residues L1005, F1012, A1017 and F1019, charged residues E1016, amphipathic residue M1008 and polar residues Q1009, T1010, T1013, T1014, T1015, N1017, Q1020 and Q1023 (Fig. 1B). The interactions of compounds with P_{HR2} occurred through hydrophobic interactions, stacking with hydrophobic rings, or hydrogen bonding. A predominant hydrogen bonding interaction was predicted with the side chain of Q1016 and backbone of A1007. Stacking interactions were observed with F1012 (Fig. 1B).

Cell-cell fusion assay

The 88 compounds with docking scores of -8.0 or higher after extra-precision docking (Supplementary Table 1) were used in the cell-cell fusion assay. The compounds were tested at a final concentration of 1 or 10 μM (Fig. 2). For cell-cell fusion assay, the compounds were evaluated and compared based on the rule that the effective compound has a cut-off score of 60% > MERS-CoV (X-axis) and 80% < Co-transfection (X-axis). Based on this rule, none of the compounds fell within the effective window at 1 μM concentration. At 10 μM, a set of compounds obeyed the presumed rule, including compound numbers 26, 33, 34, 49, 60, 61, 69, 50, and 54.

Effect of time of compounds addition of compounds on cell-cell fusion

The 88 compounds were either incubated with MERS-CoV spike expressing cells for 30 min before addition of CD26/TMPRSS2 expression cells or at the time when CD26/TMPRSS2 expression cells were added. The results indicate almost no or slight differences in cell-cell fusion inhibition. Surprisingly, there was a greater tendency to inhibit the cell-cell fusion when compounds were added promptly at zero time of the cell fusion process (Supplementary Fig. 1, Supplementary Table 2).

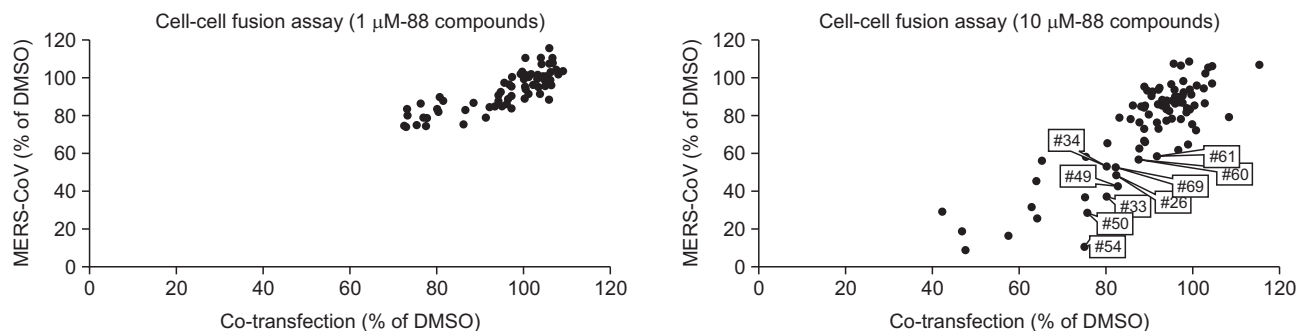
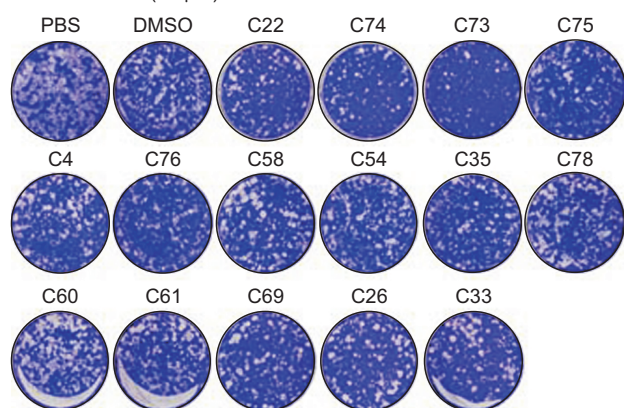


Fig. 2. The effect of 88 compounds on the cell-cell fusion assay of MERS-CoV. Each dot represents a single compound. The X-axis represents the effect of compounds on the cells co-expressing both DSP1-7 and DSP8-11 (forming active DSP); this is to elucidate the non-specific RL inhibitory activity. The Y-axis displays the effect of compounds on the DSP (RL) activity normalized to DMSO (control).

A Inhibitor set (10 μ M)



B

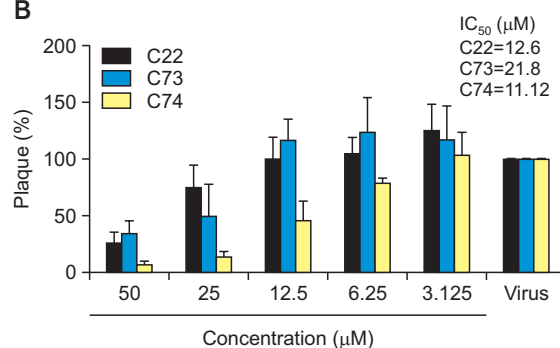


Fig. 3. (A) Screening of the inhibitors against MERS-CoV infection. The plaque formation assay was performed with 15 compounds. Prior to MERS-CoV infection, MERS-CoV was incubated with each compound (10 μ M) for 30 min at 37°C and then added to Vero cells to infect with MERS-CoV. After 4 days of incubation in DMEM/F12 containing 0.6% oxid agar, the plaques were observed by staining with crystal violet then counted. (B) Inhibitory effect of compounds 22, 73, and 74 on MERS-CoV infection in Vero cells. MERS-CoV was pre-incubated with two-fold serially diluted compounds 22, 73, or C74 ($n=3$) for 30 min at 37°C. Vero cells were treated with the mixture of the virus and each compound and incubated for 4 days in DMEM/F12 containing 0.6% oxid agar. The plaques were observed by staining with crystal violet and counted.

Plaque reduction assay

At 10 μ M concentration, 15 compounds were able to prevent MERS-CoV plaques formation by 3.3-64.5% (Table 1). The strongest compound was no. 73, which produced 74.5% reduction in MERS-CoV plaques formation. Compounds 74, 22, and 76 produced 56.2%, 44.7%, and 43% inhibition (Fig. 3). To gain more insight into the inhibitory properties of compounds, plaque assay was repeated in the presence of different concentrations of compounds 22, 73, and 74 (Supplementary Fig. 2). The final concentrations of compounds were 0, 3.125, 6.25, 12.5, 25, and 50 μ M, respectively. Results indicate the presence of a dose-dependent decrease in MERS-CoV plaques formation. The estimated IC_{50} values for compounds 22, 73, and 74 were 12.6, 21.8, and 11.12 μ M, respectively (Fig. 3B). The obtained cell-cell fusion assay data showed moderate correlation with the obtained docking score ($r=0.17$, $p=0.1$). This might be due to the presence of other factors controlling the fusion of MERS-CoV as the potential fusion through cell membrane and/or endocytosis. In comparison, there was strong correlation between the obtained

docking scores and plaques inhibition ($r=0.77$, $p=0.0007$). As the plaques assay comprises more dynamic features of virus-cell interactions, these obtained compounds are suggested to inhibit the virus infection with significant statistical confidence.

Predicted pharmacokinetic and toxicity descriptors

The effect of compounds (#22, 74, 73, 75, 4, 76, 58, 54, 35, 78, 60, 61, 69, 26, and 33) on the growth and proliferation of HEK293 cells was evaluated. Compounds 4 and 69 (20 μ M) decreased the cell numbers in HEK293 cells as evaluated by the WST1 assay (Table 1). Treatment with compound 69 slightly triggered cellular shrinking; however, each compound did not induce membrane blebbing, a typical apoptotic and/or necrotic morphological feature. Therefore, it is suggested that compounds 4 and 69 induce growth arrest but not cell death in HEK293 cells. The other compounds were not toxic against HEK293 cells.

To analyze cytotoxicity of compounds 73 and 74, we investigated their effect on growth in Vero cells using MTT assay. Vero cells exposed to the assay concentrations of compound

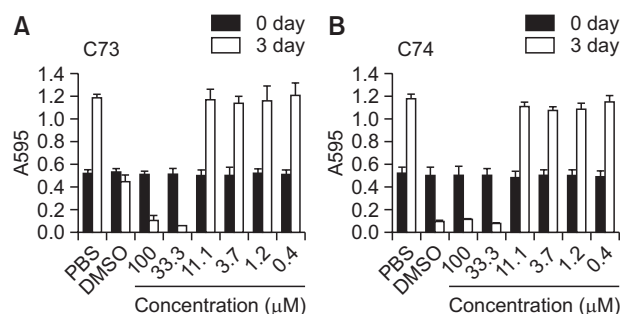


Fig. 4. Effect of compounds C73 and C74 on the growth of Vero cells. Compounds C73 and C74 (100 μM) were dissolved in 10% DMSO, and then the compounds were three-fold serially diluted in PBS. Vero cells were treated with PBS, 10% DMSO, indicated concentration of C73 (A) or C74 (B) for 3 days followed by the MTT assay.

73 and 74 (10 μM) showed no cytotoxicity (Fig. 4). Therefore, the inhibitory effect of the compounds is not related with toxicity of the compounds. However, high concentration of 73 and 74 treatment reduced the growth of Vero cells. Considering that we dissolved the peptides in 10% DMSO and then serially diluted them in PBS, the reduced growth can be attributed to the toxic effect of DMSO at a high concentration (confirmed experimentally).

The drug-likeness, predicted pharmacokinetic, and toxicity descriptors are provided in Supplementary Table 3. All compounds showed no or ≤ 2 violations of Lipinski's rule of five. All of the compounds exhibited acceptable ranges for aqueous solubility, IC_{50} value for blockage of HERG K⁺ channels, number of rotatable bonds, binding to human serum albumin, and solvent accessible surface area with hydrophilic component of the SASA with predicted high cell permeability of Caco-2 and MDCK cells. Compounds 73 and 74 showed negative values for the carcinogenicity test in rats and mice as well as negative values with the Ames toxicity test.

DISCUSSION

Despite the emerging and fatal nature of MERS-CoV, structure-based drug discovery studies against this virus are very limited. Computational studies have largely contributed to the drug discovery process, especially through lead identification and optimization (Kirchmair *et al.*, 2011). Small molecules inhibitors against several MERS-CoV targets were provided to the research community (Galasiti Kankanamalage *et al.*, 2018; Kandeel *et al.*, 2019; Lee *et al.*, 2019; Rahman *et al.*, 2019; Shen *et al.*, 2019).

In this study, a trial was designed to discover new MERS-CoV fusion inhibitors, which was initialized by a virtual screening campaign of 1.2 million compounds. A set of initial drug candidates was obtained based on docking score and visual examination of the binding mode. Further analysis by *in vitro* assays confirmed their inhibitory properties on a MERS-CoV spike fusion. In addition, a significant decrease in MERS-CoV plaque formation suggests the accepted general inhibitory effect of these new compounds on MERS-CoV replication.

The obtained compounds with high docking scores demonstrated the predicted local hydrophilic interactions with HR1

helices comparable to its counter-partner protein in HR2. The HR2 helix interacts with HR1 helices by hydrogen bonds only at its N and C termini (Lu *et al.*, 2014). Most of the 15 compounds listed in Table 1 formed at least one hydrogen bond, primarily with N1016, which is centered in P_{HR2} facing the center of HR2 helix. Therefore, these compounds provide combined hydrophobic and hydrophilic interactions through their hydrophobic rings and charged moieties with a unique feature of interactions with the center of P_{HR2} . Computational competency of the predicted compounds, regarding their favorable pharmacokinetic descriptors, supports their drug-likeness properties.

Pre-incubation of the compounds with MERS-CoV spike expression cells for 30 min before adding DPP4 receptors expression cells did not significantly inhibit cell-cell fusion compared with adding the compounds at the time of cell-cell interactions. However, the addition of compounds at the start of fusion process over the pre-incubation of cells expressing the MERS-CoV spike resulted in a slight tendency to affect DSP activity and inhibit cell-cell fusion. In absence of the spike-receptor interaction and due to the disorganization of the cavity hosting the compounds, the partially unfolded S2 protein cannot host the compounds. The formation of the predetermined drug binding cavities on S2 might be activated the moment the spike-receptor interaction initiates. This agrees with the main concept of fusion inhibitors, which act only during the early stages of viral infection (Lundin *et al.*, 2010; Xu *et al.*, 2019).

Except for 4 and 69, no other compounds (20 μM) induced apparent morphological changes and damages in HEK293 cells. In parallel, the WST1 values indicating cell proliferation and damages were hardly influenced by 25 h of treatment with each compound. Cytotoxicity assays indicate the general safety of the compounds in the low micromolar range.

In the search for new anti-MERS-CoV agents, a MERS-CoV fusion protein was targeted using a structure-based approach. This study introduces the first set of compounds that can bind to cavities at the surface of the MERS-CoV fusion core and capable to inhibit viral fusion and MERS-CoV plaque formation. The compounds were found as a promising lead structure that fits well with pockets on the MERS-CoV fusion protein. About 10 compounds were effective in reducing MERS-CoV plaques by more than 30% at 10 μM concentration, and three compounds (no. 22, 73, and 74) with IC_{50} of 11.12-12.6 μM displayed potent inhibition. The present set of compounds is considered as lead structures and provides a basis for future drug discovery studies and development of MERS-CoV anti-viral agents.

CONFLICT OF INTEREST

None.

ACKNOWLEDGMENTS

The authors acknowledge the Deanship of Scientific Research at King Faisal University for the financial support under Strategic projects track (Grant No. 171001). Hyung-Joo Kwon was supported by grants from the National Research Foundation (2016M3A9B6916708) funded by the Ministry of Science and ICT in the Republic of Korea. This work was sup-

ported in part by grants-in-aid from the Ministry of Education, Culture, Sports, Science, and Technology, Japan (16H06575 to JI), from the Japan Society for the Promotion of Science [18K15235 to MY, 16H06276 AdAMS) to J.I.], and by the Japan Agency for Medical Research and Development (AMED) [Program of Japan Initiative for Global Research Network on Infectious Diseases (JGRID) JP18fm0108006 to MY and JI].

REFERENCES

- Bosch, B. J., van der Zee, R., de Haan, C. A. and Rottier, P. J. (2003) The coronavirus spike protein is a class I virus fusion protein: structural and functional characterization of the fusion core complex. *J. Virol.* **77**, 8801-8811.
- Chan, J. F., Lau, S. K., To, K. K., Cheng, V. C., Woo, P. C. and Yuen, K. Y. (2015) Middle East respiratory syndrome coronavirus: another zoonotic betacoronavirus causing SARS-like disease. *Clin. Microbiol. Rev.* **28**, 465-522.
- Cho, S. Y., Kang, J. M., Ha, Y. E., Park, G. E., Lee, J. Y., Ko, J. H., Lee, J. Y., Kim, J. M., Kang, C. I., Jo, I. J., Ryu, J. G., Choi, J. R., Kim, S., Huh, H. J., Ki, C. S., Kang, E. S., Peck, K. R., Dhong, H. J., Song, J. H., Chung, D. R. and Kim, Y. J. (2016) MERS-CoV outbreak following a single patient exposure in an emergency room in South Korea: an epidemiological outbreak study. *Lancet* **388**, 994-1001.
- Friesner, R. A., Banks, J. L., Murphy, R. B., Halgren, T. A., Klicic, J. J., Mainz, D. T., Repasky, M. P., Knoll, E. H., Shelley, M., Perry, J. K., Shaw, D. E., Francis, P. and Shenkin, P. S. (2004) Glide: a new approach for rapid, accurate docking and scoring. 1. Method and assessment of docking accuracy. *J. Med. Chem.* **47**, 1739-1749.
- Galasiti Kankanamalage, A. C., Kim, Y., Damalanka, V. C., Rathnayake, A. D., Fehr, A. R., Mehzabeen, N., Battaile, K. P., Lovell, S., Lushington, G. H., Perlman, S., Chang, K. O. and Groutas, W. C. (2018) Structure-guided design of potent and permeable inhibitors of MERS coronavirus 3CL protease that utilize a piperidine moiety as a novel design element. *Eur. J. Med. Chem.* **150**, 334-346.
- Gao, J., Lu, G., Qi, J., Li, Y., Wu, Y., Deng, Y., Geng, H., Li, H., Wang, Q., Xiao, H., Tan, W., Yan, J. and Gao, G. F. (2013) Structure of the fusion core and inhibition of fusion by a heptad repeat peptide derived from the S protein of Middle East respiratory syndrome coronavirus. *J. Virol.* **87**, 13134-13140.
- Halgren, T. A., Murphy, R. B., Friesner, R. A., Beard, H. S., Frye, L. L., Pollard, W. T. and Banks, J. L. (2004) Glide: a new approach for rapid, accurate docking and scoring. 2. Enrichment factors in database screening. *J. Med. Chem.* **47**, 1750-1759.
- Huang, X., Li, M., Xu, Y., Zhang, J., Meng, X., An, X., Sun, L., Guo, L., Shan, X., Ge, J., Chen, J., Luo, Y., Wu, H., Zhang, Y., Jiang, Q. and Ning, X. (2019) Novel gold nanorod-based HR1 peptide inhibitor for Middle East respiratory syndrome coronavirus. *ACS Appl. Mater. Interfaces* **11**, 19799-19807.
- Kandeel, M., Al-Taher, A., Li, H., Schwingenschlogl, U. and Al-Nazawi, M. (2018) Molecular dynamics of Middle East Respiratory Syndrome Coronavirus (MERS CoV) fusion heptad repeat trimers. *Comput. Biol. Chem.* **75**, 205-212.
- Kandeel, M., Altaher, A. and Alnazawi, M. (2019) Molecular dynamics and inhibition of MERS CoV papain-like protease by small molecule imidazole and aminopurine derivatives. *Letf. Drug Des. Disc.* **16**, 584-591.
- Kandeel, M., Elaiziz, M., Kandeel, A., Altaher, A. and Kitade, Y. (2014) Association of host tropism of Middle East syndrome coronavirus with the amino acid structure of host cell receptor dipeptidyl peptidase 4. *Acta Virol.* **58**, 359-363.
- Kim, Y., Cheon, S., Min, C. K., Sohn, K. M., Kang, Y. J., Cha, Y. J., Kang, J. I., Han, S. K., Ha, N. Y., Kim, G., Aigerim, A., Shin, H. M., Choi, M. S., Kim, S., Cho, H. S., Kim, Y. S. and Cho, N. H. (2016) Spread of mutant Middle East respiratory syndrome coronavirus with reduced affinity to human CD26 during the South Korean outbreak. *MBio* **7**, e00019.
- Kirchmair, J., Distinto, S., Liedl, K. R., Markt, P., Rollinger, J. M., Schuster, D., Spitzer, G. M. and Wolber, G. (2011) Development of anti-viral agents using molecular modeling and virtual screening techniques. *Inf. Disord. Drug Targets* **11**, 64-93.
- Lee, H., Ren, J., Pesavento, R. P., Ojeda, I., Rice, A. J., Lv, H., Kwon, Y. and Johnson, M. E. (2019) Identification and design of novel small molecule inhibitors against MERS-CoV papain-like protease via high-throughput screening and molecular modeling. *Bioorg. Med. Chem.* **27**, 1981-1989.
- Lu, L., Liu, Q., Zhu, Y., Chan, K. H., Qin, L., Li, Y., Wang, Q., Chan, J. F., Du, L., Yu, F., Ma, C., Ye, S., Yuen, K. Y., Zhang, R. and Jiang, S. (2014) Structure-based discovery of Middle East respiratory syndrome coronavirus fusion inhibitor. *Nat. Commun.* **5**, 3067.
- Lundin, A., Bergström, T., Bendrioua, L., Kann, N., Adamiak, B. and Trybala, E. (2010) Two novel fusion inhibitors of human respiratory syncytial virus. *Antiviral Res.* **88**, 317-324.
- Memish, Z. A., Zumla, A. I., Al-Hakeem, R. F., Al-Rabeeah, A. A. and Stephens, G. M. (2013) Family cluster of Middle East respiratory syndrome coronavirus infections. *N. Engl. J. Med.* **368**, 2487-2494.
- Oh-hashii, K., Soga, A., Naruse, Y., Takahashi, K., Kiuchi, K. and Hirata, Y. (2018) Elucidating post-translational regulation of mouse CREB3 in Neuro2a cells. *Mol. Cell. Biochem.* **448**, 287-297.
- Park, B. K., Maharjan, S., Lee, S. I., Kim, J., Bae, J. Y., Park, M. S. and Kwon, H. J. (2019) Generation and characterization of a monoclonal antibody against MERS-CoV targeting the spike protein using a synthetic peptide epitope-CpG-DNA-liposome complex. *BMB Rep.* **52**, 397-402.
- Rahman, A. and Sarkar, A. (2019) Risk factors for fatal Middle East respiratory syndrome coronavirus infections in Saudi Arabia: analysis of the WHO line list, 2013-2018. *Am. J. Public Health* **109**, 1288-1293.
- Rahman, M. M., Hosen, M. B., Howlader, M. Z. H. and Kabir, Y. (2019) Lead molecule prediction and characterization for designing MERS-CoV 3C-like protease inhibitors: an in silico approach. *Curr. Comput. Aided Drug Des.* **15**, 82-88.
- Shen, L., Niu, J., Wang, C., Huang, B., Wang, W., Zhu, N., Deng, Y., Wang, H., Ye, F., Cen, S. and Tan, W. (2019) High-throughput screening and identification of potent broad-spectrum inhibitors of coronaviruses. *J. Virol.* **93**, e00023-19.
- Su, S., Wong, G., Liu, Y., Gao, G. F., Li, S. and Bi, Y. (2015) MERS in South Korea and China: a potential outbreak threat? *Lancet* **385**, 2349-2350.
- Sun, Y., Zhang, H., Shi, J., Zhang, Z. and Gong, R. (2017) Identification of a novel inhibitor against Middle East respiratory syndrome coronavirus. *Viruses* **9**, E255.
- Wang, C., Xia, S., Zhang, P., Zhang, T., Wang, W., Tian, Y., Meng, G., Jiang, S. and Liu, K. (2018) Discovery of hydrocarbon-stapled short alpha-helical peptides as promising Middle East respiratory syndrome coronavirus (MERS-CoV) fusion inhibitors. *J. Med. Chem.* **61**, 2018-2026.
- Wang, H., Li, X., Nakane, S., Liu, S., Ishikawa, H., Iwamoto, A. and Matsuda, Z. (2014) Co-expression of foreign proteins tethered to HIV-1 envelope glycoprotein on the cell surface by introducing an intervening second membrane-spanning domain. *PLoS ONE* **9**, e96790.
- Wang, N., Shi, X., Jiang, L., Zhang, S., Wang, D., Tong, P., Guo, D., Fu, L., Cui, Y., Liu, X., Arledge, K. C., Chen, Y. H., Zhang, L. and Wang, X. (2013) Structure of MERS-CoV spike receptor-binding domain complexed with human receptor DPP4. *Cell Res.* **23**, 986-993.
- Xia, S., Liu, Q., Wang, Q., Sun, Z., Su, S., Du, L., Ying, T., Lu, L. and Jiang, S. (2014) Middle East respiratory syndrome coronavirus (MERS-CoV) entry inhibitors targeting spike protein. *Virus Res.* **194**, 200-210.
- Xu, W., Pu, J., Su, S., Hua, C., Su, X., Wang, Q., Jiang, S. and Lu, L. (2019) Revisiting the mechanism of enfuvirtide and designing an analog with improved fusion inhibitory activity by targeting triple sites in gp120. *AIDS* **33**, 1545-1555.
- Yamamoto, M., Matsuyama, S., Li, X., Takeda, M., Kawaguchi, Y., Inoue, J. I. and Matsuda, Z. (2016) Identification of nafamostat as a potent inhibitor of Middle East respiratory syndrome coronavirus S protein-mediated membrane fusion using the split-protein-based cell-cell fusion assay. *Antimicrob. Agents Chemother.* **60**, 6532-6539.